Nano-frictional investigation on boundary lubricity of oleic acid, methyl oleate and trimethylolpropane trioleate

Chiew Tin Lee [1*], Mei Bao Lee [1], William Woei Fong Chong [1,2], Syahrullail Samion [1]

[1] School of Mechanical Engineering, Faculty of Engineering, Universiti Teknologi Malaysia, 81310 UTM Skudai, Johor, MALAYSIA.
[2] Automotive Development Centre (ADC), Institute of Vehicle Systems and Engineering (IVeSE), Universiti Teknologi Malaysia, 81310 UTM Skudai, Johor, MALAYSIA.
*Corresponding author: ctlee5@graduate.utm.my

1.0   INTRODUCTION

Vegetable oil is known to have good lubrication properties due to its ester functionality (Odi-Owei, 1989). The highly polar carboxyl (COOH-) group of the fatty acid chain interacts with the metallic surface by physical adsorption, hence, sticking on the surface. Consequently, the non-polar alkyl group (CH-) of the fatty acid then forms the free end further from the metallic surface, forming a "brush-like" barrier to separate opposing surfaces apart that often results in reduced friction (Aziz et al., 2016; Jiang et al., 2015). Such a friction-reducing trend has been reported by Kržan and Vižintin (2003), where they found that rapeseed oil and high oleic sunflower oil exhibited a low coefficient of friction (CoF) as compared to mineral oil-based lubricant. However, they also observed that the wear of surfaces lubricated by the tested vegetable oil is higher when compared with mineral oil.

In a separate study, Rani et al. (2015) compared the tribological properties of various vegetable oils (rice bran oil, sunflower oil and coconut oil) with SAE20W40 grade lubricant. Both rice bran oil (0.073) and sunflower oil (0.060) showed a low coefficient of friction (CoF) values, while coconut oil (0.101) and SAE20W40 (0.117) gave higher CoF values. The authors explained that the varying friction performance among the vegetable oil samples was attributed to the different chain lengths. For example, coconut oil mainly comprises short chains (between C8 and C14), while rice bran oil and sunflower oil consist of a longer chain length (mainly C18). As the carbon chain length increases, the adsorption ability of the molecule to form boundary adsorbed film also increases, providing a more effective molecular barrier (Zulkifli et al., 2014, 2016). Even though rice bran oil has better frictional properties when compared with SAE20W40, it still exhibited high chemical wear due to the presence of free fatty acids.

The phenomenon, where friction is reduced but at the expense of higher wear experienced by vegetable oil lubricated contacts, is attributed to the low bonding stability between the oxide layer and the organic acid, resulting in low shear strength adsorbed film. Besides, vegetable oil also has low thermal-oxidation stability that limits its range of application. Therefore, the chemical modification of vegetable oil into an improved form of ester has often been adopted to overcome this weakness. Through chemical modifications, the formation of ester linkage in the molecule increases its polarity, thus, strengthening the boundary adsorbed film (Shashidhara and Jayaram, 2010; Rudnick, 2005). A type of chemical modification method for vegetable oil is transesterification. The commonly adopted first stage of transesterification of vegetable oil in the presence of a catalyst and alcohol (methanol) produces fatty acid methyl esters (FAME) or biodiesel (see Figure 1(a)) (Hamdan et al., 2018).

It has been widely reported that FAME exhibits an enhanced lubricity as compared to its original fatty acid self. A study conducted by Fazal et al. (2013) showed that the presence of fatty acid composition of FAME could reduce both friction and wear of steel ball in a four-ball test. Both friction and wear decreased as the content of FAME are increased. However, the low viscosity nature of FAME has limited its use mainly as a fuel alternative to petro-diesel. To elevate the viscosity to be suitable as a lubricant, the second stage of transesterification can be conducted (see Figure 1(b)). As an example, Sripada et al. (2013) synthesised trimethylolpropane (TMP)-based biolubricant from methyl oleate and canola biodiesel. The three branched long alkyl groups of polyols TMP form a more stable synthesis ester (TMP ester) when compared with FAME. It prevents the self-polymerisation in FAME, thus, enhances its thermal oxidation stability with superior load-carrying capacity (Mahmud et al., 2015; Zulkifli et al., 2016). Therefore, TMP ester has been shown to provide a better lubrication characteristic than its initial state or FAME.
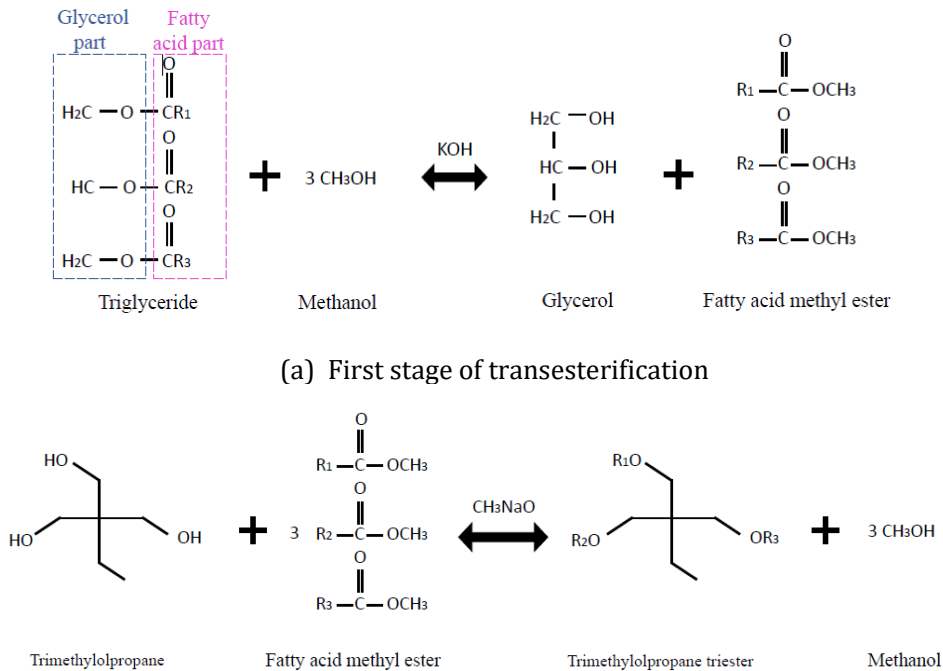
(a) First stage of transesterification

(b) Second stage of transesterification
Figure 1: transesterification of vegetable oil into synthesis ester.
Note: *R= alkyl group (C_nH_{2n+1})

Apart from focusing on the parameter of CoF and wear scar diameter, it is also imperative to understand the fundamental principle governing the shear of such a boundary adsorbed film. When under shear, a molecule needs to gain a certain amount of energy to overcome a potential barrier for continuous sliding motion. The abovementioned potential barrier can be interpreted through a thermal activation model introduced by Eyring (1936). Eyring assumed that the energy barrier reduces while equal external work is done on the system. He claimed that externally applied force accelerates the rate of thermal transition of a molecule across the energy barrier present in solid and liquid material, thus, promoting flow, slip or bond cleavage. For example, Briscoe and Evans (1982) studied the influence of sliding speed, applied load and temperature on the boundary friction of Langmuir-Blodgett monolayers of a range of fatty acids and fatty acid soaps across mica-covered glass by interpreting their results using Eyring's model. They found good agreement between the equation and experimental measurements. Briscoe and Evans also found that monolayers of free fatty acids gave smooth friction that increases linearly with the log of sliding speed at a given load. Recently, Eyring's model is also used to interpret lateral force measurements via Atomic Force Microscopy (AFM) (Chong and Rahnejat, 2015; Chong and Ng, 2016; Hamdan et al. 2021).

Subhalakshmi et al. (2008) investigated the link between the frictional performance of two test molecules, perfluroocytltrichlorosilane (FOST) and octadecyltrichlorosilane (ODTS), on a silicon wafer and thermal activation energy parameters. The analysis was performed by varying the normal load, temperature and sliding velocity before further analysing the Eyring equation.

The CoF for FOST (-CF3) is three times greater than ODTS (-CH3), and the corresponding difference is also reflected through the larger barrier energy for FOST. Their results showed that when two molecules are well-packed, shear coordination modulates the different frictional behaviour, thus, causing a distinction in activation energy to initiate sliding, Q.

Vegetable-oil-based biolubricant has been introduced to substitute fossil fuel-based lubricant due to its high biodegradability and renewability. Comparative studies have been carried out to investigate the tribological properties of various stages of transesterified vegetable-oil-based biolubricant, namely vegetable oil (Ranjan et al., 2021), methyl ester (Pandey et al., 2020 ; Shahabuddin et al., 2020) and synthesis ester (e.g., TMP ester) (Wafti et al., 2021), individually. However, it remains a question as to which stage of vegetable-oil-based biolubricant might be relevant for different types of lubrication purposes. Also, most of the studies emphasised the friction and wear performances of these biolubricant as an alternative to existing commercial lubricants rather than the mechanisms that impart lubricity, especially at boundary lubrication regimes (Srinivas et al., 2020; Yunus et al., 2020.

Although Eyring's model was initially derived to explain liquid viscosity, it can also be interpreted in the relation of sliding velocity with shear stress among the boundary layer as it is based on the movement of molecules in acquiring the activation energy to slip across its potential barrier to its neighbour (Eyring, 1936). The analysis based on Eyring thermal activation model is expected to be able to improve the understanding of the mechanism of dissipation involved in sliding of a boundary fluid layer, thus, providing a suitable method in selecting boundary lubricants with objective assumptions (Overney et al., 2004; Briscoe and Evans, 1982; McDermott et al., 1997).

Therefore, as an initial approximation, this paper aims to interpret the nano-frictional characteristics among the oleic family, named oleic acid, methyl oleate and TMP trioleate using the thermal activation energy model as explained by Chong and Rahnjeat (2015). The nano-friction is to be measured using Lateral Force Microscopy (LFM), allowing for the isolation of the boundary shear strength for the investigated lubricant types.

2.0   EXPERIMENTAL PROCEDURE

2.1   Sample Preparation

In the present study, oleic acid and methyl oleate were obtained from Sigma-Aldrich while TMP trioleate was procured from Wilmar (China) Oleo Co., Ltd. Figure 2 shows the differences among the oleic family in their respective molecular structure. Oleic acid has a double bond with the tail end of the hydrogen bond (-OH). Methyl oleate can be obtained through the chemical process of oleic acid and forming a new ester structure by reacting fatty acyl group of oleic acid with an alcohol. In contrast, transesterification of trimethylolpropane (TMP) and three methyl oleate molecules produce TMP trioleate. This chemical modification is the reverse transesterification process by replacing the alcohol of methyl oleate with TMP, hence, TMP trioleate is a branched ester that is much heavier in molecular weight than oleic acid and methyl oleate.

(a)Oleic acid

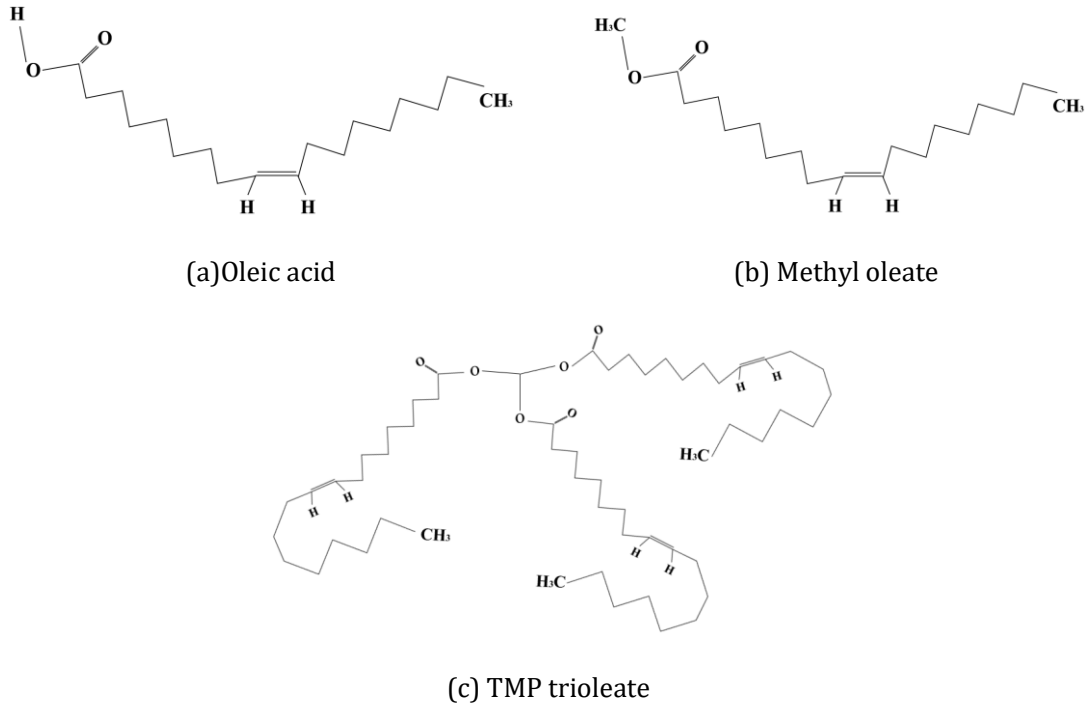(b) Methyl oleate

(c) TMP trioleate

Figure 2: Molecular structure of the oleic family.

The AFM cantilever tip was purchased from Park System (PPP-CONTSCR). A 1 cm x 1 cm stainless steel substrate (SUS304) was used as the sliding surface for the tested fluids. The surface samples were mirror-polished, with roughness parameters, Sq of approximately 0.9 nm. Since the Sq is smaller than the AFM tip radius (≈10 nm), the effect of surface roughness is negligible when measuring the frictional properties. Before each lateral force test, the surface of the samples was cleaned using an alcohol pad and left to dry in a desiccator. Before conducting the friction tests, the viscosity of the test fluids was measured along with their thermal decomposition properties measured using thermogravimetric analysis (TGA) under ambient conditions.

2.2   Lateral Force Microscopy (LFM)

The boundary friction was measured using a commercial Lateral Force Microscopy (LFM) (Park System XE-7 AFM), coupled with the fluid imaging given in Figure 3. The experiment was carried out for a normal load between 1 nN and 10 nN with the sliding velocity of the cantilever tip (named AFM tip), in the range of 2 μm/s to 200 μm/s. The LFM measurement was initiated by scanning the dry condition of each sample. Then, the tested fluid was added slowly between the contact. During the fluid imaging approach setup, an inlet meniscus must be observed around the liquid probe holder, ensuring a full submersion of the AFM tip in the test fluid (see Figure 3). This precautionary step was required to eliminate the influence of meniscus forces on friction testing. A large negative meniscus pressure existing along the edge of the tip holder and fluid tested can keep the meniscus further away from the tip, guarding it against adhesion of the cantilever during the LFM measurement (Leighton et al., 2017).
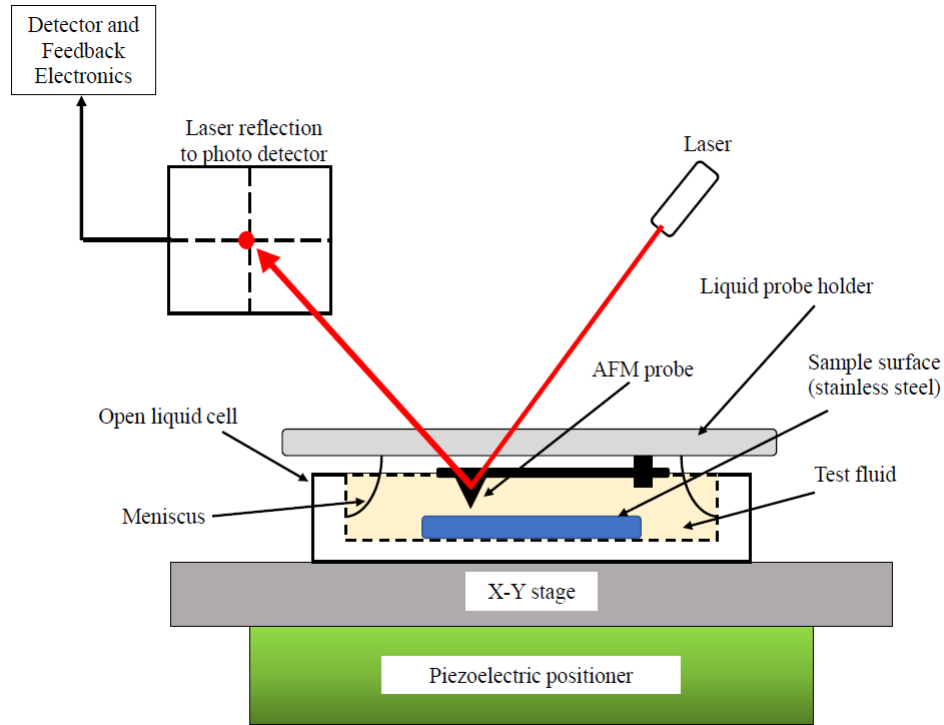
Figure 3: LFM setup with fluid imaging.

2.2.1 LFM Calibration Method

The properties of the AFM tip were calibrated using a standard silicon wafer piece with a known coefficient of boundary shear strength of 0.19±0.1 (Ahimou et al., 2007). The LFM measurements for each test fluid were conducted using a new AFM tip. From the lateral force measurement, the average tangential friction force, F_f value, was obtained from the trace-and-retrace data recorded in each scan at its respective applied normal load. Since the output trace and retrace data were in voltage signal, the Blind calibration approach, proposed by Buenviaje et al. (1998), was adopted for the conversion of electrical signal (nV) into physical friction value (nN). The calibration factor for the AFM tip on a silicon calibration sample can be determined as Eq. 1.:

$$\alpha = \frac{F_f\,(v)\big/F_n(nN)}{0.19} \tag{1}$$

Where α is the calibration factor for each AFM tip, and the value of 0.19 was used as the coefficient of boundary shear strength of silicon wafer. The calculated α values were then curve-fitted with the best power curve to obtain the respective α values. By using this calibration factor, the friction force was then converted into physical parameter using the Eq. 2.:

$$F_n\,(nN) = \frac{F_f\,(v)}{a_{eqn}\,(V/nN)} \tag{2}$$

6

2.3   EYRING THERMAL ACTIVATION ENERGY

During sliding motion, all molecules need to overcome an energy barrier to maintain continuous sliding motion. The molecular interactions then form an energy barrier through contact pressure and shearing action. The potential energy barrier, E based on the Eyring thermal activation energy model is expressed as Eq. 3 (see Figure 4):

$$E = Q + P\Omega - \tau\phi \qquad (3)$$

where:
ϕ = shear activation volume,
Ω = pressure activation volume,
Q = activation energy to initiate sliding,
P = contact pressure, and
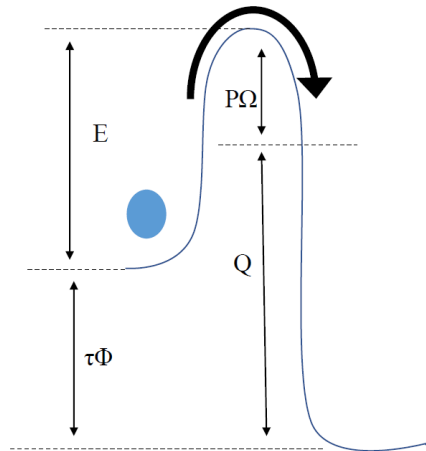τ = shear stress

Figure 4: Schematic diagram of Eyring thermal activation energy model.

Assuming the average time for an individual molecule to pass through its potential barrier process to conform with the Boltzmann distribution, the shear stress, τ of the Eyring "cage" model can be written as in Eq. 4. The Eyring equation shows the potential energy barrier, E increases with P but reduces with τ (see Eq. 3). Also, Eq. 4 demonstrates the linear relationship of τ, P and temperature, T. These activation energy components might result in a positive or negative value, depending on the state of thermal equilibrium of the molecules (Briscoe and Evans, 1982; Chong and Rahnejat, 2015; Hamdan et al., 2018; Spikes, 2018).

$$\tau = \frac{k_B T}{\phi}\ln(\frac{v}{v_0}) \; + \; \frac{1}{\phi}\,(Q + P\Omega) \qquad (4)$$

where:
k_B = Boltzmann constant (J/(mol.K)),
T = temperature (K),
v_0 = characteristic constant velocity, and
v = sliding speed

The term v_0 has been suggested to be 20 μm/s from the literature based on the combination of molecule vibration frequency and the lattice constant. (Briscoe and Evans, 1982). To determine the other activation energy components in this study, Eq. 4 is differentiated with respect to the sliding speed, ln v. Rearranging the differential equation, ϕ would then result in Eq. 5. The polynomial curve-fit equation obtained from τ vs ln v is also differentiated to determine the instantaneous value of θ to calculate ϕ.

$$\phi = \frac{k_B T}{\theta} \qquad (5)$$

where,

$$\theta = \frac{\partial \tau}{\partial (\ln v)} \qquad (6)$$

Furthermore, the Eyring equation can be expressed in terms of τ and P at a constant T and v, as shown in Eq. 7 by taking τ_0 as the y-intercept of the graph. The pressure activation volume, Ω can then be obtained through Eq. 8.

$$\tau = \alpha P + \tau_0 \qquad (7)$$

$$\alpha = \frac{\Omega}{\phi} \qquad (8)$$

Using the described method above, all activation energy components of E, Q, $P\Omega$ and $\tau\phi$ for tested fluids can be calculated with Q being determined using Eq. 4. The thermal activation energy components are expected to provide the information for each fluid molecule's behaviour as well as stress and pressure activation volume (structure parameters) that can be correlated with its respective frictional characterisation.

3.0   RESULTS AND DISCUSSION

Before the frictional properties were measured, the kinematic viscosity and thermal decomposition behaviour of the tested fluids were determined. The onset temperature was determined using thermogravimetric analysis (TGA) at a heating rate of 10°C/min. The thermogravimetric (TG) and derivative thermogravimetric (DTG) curves were plotted in Figure 5. Following DIN EN ISO 11357-1, the extrapolated onset temperature for each tested fluid was determined in Table 1 along with the respective kinematic viscosity values. Aside from being the most viscous, it can be observed that the onset temperature, where decomposition began to occur, for TMP trioleate was the highest among the tested fluids. Interestingly, this onset temperature range is comparable to the commercial SAE10W30 engine oil (218 °C) (Bongfa et al., 2020). Figure 5(b) explains the thermal behaviour of each test fluid. The thermal degradation depends on the molecular structure, such as double bond, linear or branched structure and impurities, in the test fluid. TMP trioleate is synthesised through transesterification and forms a branched ester with the combination of three methyl oleates. TMP trioleate is a much larger molecule as compared to oleic acid and methyl oleate, where both are linear fatty acids with a single double bond. Hence, TMP trioleate is shown to degrade at a higher temperature at 230°C. This observation follows the findings reported by Yunus et al. (2020).
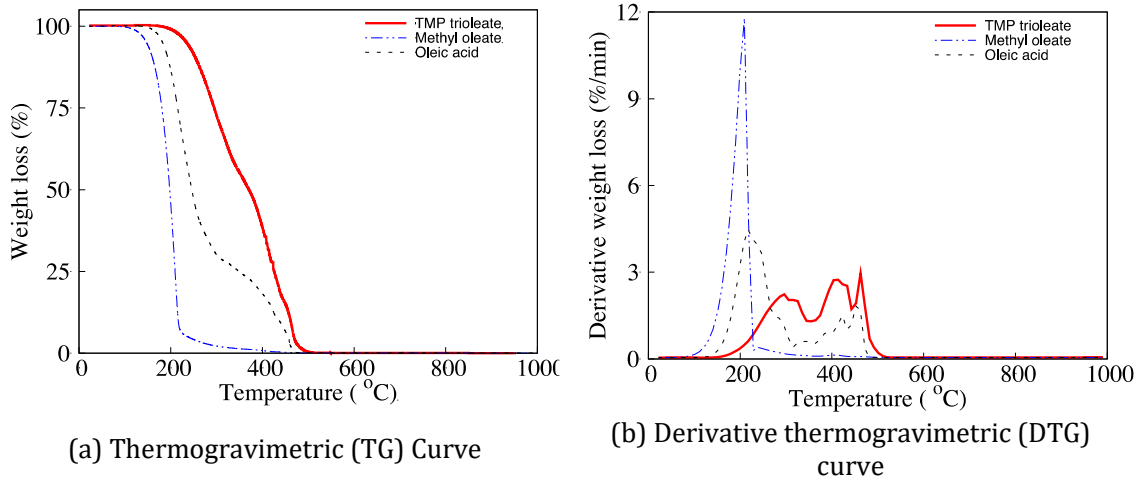
(a) Thermogravimetric (TG) Curve

(b) Derivative thermogravimetric (DTG) curve

Figure 5: Thermogravimetric analysis for tested fluids.

Table 1: Viscosity and onset temperature for tested fluids.

Type of fluid	Kinematic Viscosity (mm^2/s) @40°C	Onset Temperature (°C)
TMP trioleate	55.7	230
Methyl oleate	6.1	172
Oleic acid	20.0	181

Upon identifying the difference in rheological properties, the friction force was measured as in Figure 6. For most conditions, the friction forces were measured to increase linearly with increasing applied normal load at AFM tip sliding velocities. Previous studies have also observed similar trends (Briscoe and Evans, 1982; Subhalakshmi et al., 2008; Umer et al., 2020; Hamdan et al., 2018). Between 2 μm/s and 100 μm/s, methyl oleate produced the highest friction force, followed by oleic acid and TMP trioleate. At 200 μm/s, the measured frictions for the tested fluids were quite similar, except at a higher applied normal load of 10 nN, with oleic acid exhibiting the least desirable friction.

Figure 7 further illustrates the coefficient of friction (CoF) of the tested fluids across the range of sliding speeds measured. Typically, under Newtonian assumption, it is expected that TMP trioleate with higher viscosity to possess higher viscous shear. However, overall, TMP trioleate exhibited the lowest CoF across the range of tested speeds, except at 200 μm/s. This is because for the current study, the LFM measurements are conducted at boundary lubrication regime, where non-Newtonian behaviour is expected to prevail. It is interesting to note that as the sliding speed increases, the CoF of methyl oleate decreases while TMP trioleate and oleic acid experience gradual increments.

To elucidate such an observed frictional behaviour, the study adopted the Eyring thermal activation energy model. The measured friction forces at their respective applied normal loads were first converted to shear stresses and compressive contact pressures. Since adhesion work is negligible in wet condition during friction measurement and friction is expected to be dominated by its sliding motion, hence, the study assumed a Hertzian contact, A as follow:

$$A = \pi(\frac{3F_nR}{4E^*})^{2/3} \tag{10}$$

where:
F_n = applied normal loads
R = radius of the AFM tip ($\approx$10nm), and
E^*= effective elastic modulus

$$E^* = \frac{1}{\frac{1 - v_1^2}{E_1} + \frac{1 + v_2^2}{E_2}} \tag{11}$$

From Eq. 11, the effective elastic modulus, E^* was computed as 128.80 GPa by taking E_1= 297 GPa and v_1 = 0.28 (Chong and Ng, 2016) for silicon nitrate and E_2 = 210 GPa and v_2 = 0.27 for stainless steel sample (Hamdan et al., 2021). For applied loads between 1 nN and 10 nN, the peak Hertzian pressure can then be determined to be between 3.25 GPa and 6.99 GPa. Such values of peak Hertzian pressure allow for the contact to operate at boundary lubrication regime (Hamrock et al. 2004). The calculated contact area is further used to interpret shear stress, $\tau = F_f/A$ and contact pressure, $P = F_n/A$.

Table 2 summarises the averaged thermal activation energy components for the tested fluids based on the Eyring model. It is interesting to note that the potential energy barrier, E (based on Eq. (3)), is near identical for all the tested fluids. However, the activation energy components for these fluids differed from each other significantly, giving rise to the varying potential mechanisms underlying their frictional characteristics. Referring to Figure 4, the potential energy barrier, E, is the energy required to initiate sliding of a molecule, while Q is influenced by the pressure activation energy ($P\Omega$) and shear activation energies ($\tau\phi$).

The pressure activation energy ($P\Omega$) has been identified as the ability of a molecule to withstand the applied load (Chong and Ng, 2016). From Table 2, it can be observed that the TMP trioleate has the largest load carrying capacity (highest $P\Omega$). This can be explained by its closely packed and relatively larger molecular size of TMP trioleate than the other test fluids. Previous studies indicated that closely packed molecular structure could strengthen their Van der Waal forces, forming a stronger boundary film (Jahanmir and Beltzer, 1986). Evidently, such a characteristic resulted in TMP trioleate having the lowest measured friction force for most of the tested velocities, except at 200µm/s. On the contrary, the stronger Van der Waal forces between the molecules might have also attributed to the attractive/adhesive nature of the activation energy to initiate sliding (Q) found for TMP trioleate before continuous sliding commences. Consequently, a higher shear activation energy ($\tau\phi$) is also required for TMP trioleate to maintain continuous sliding.

(a) 2 µm/s

(b) 10 µm/s

(c) 20 µm/s
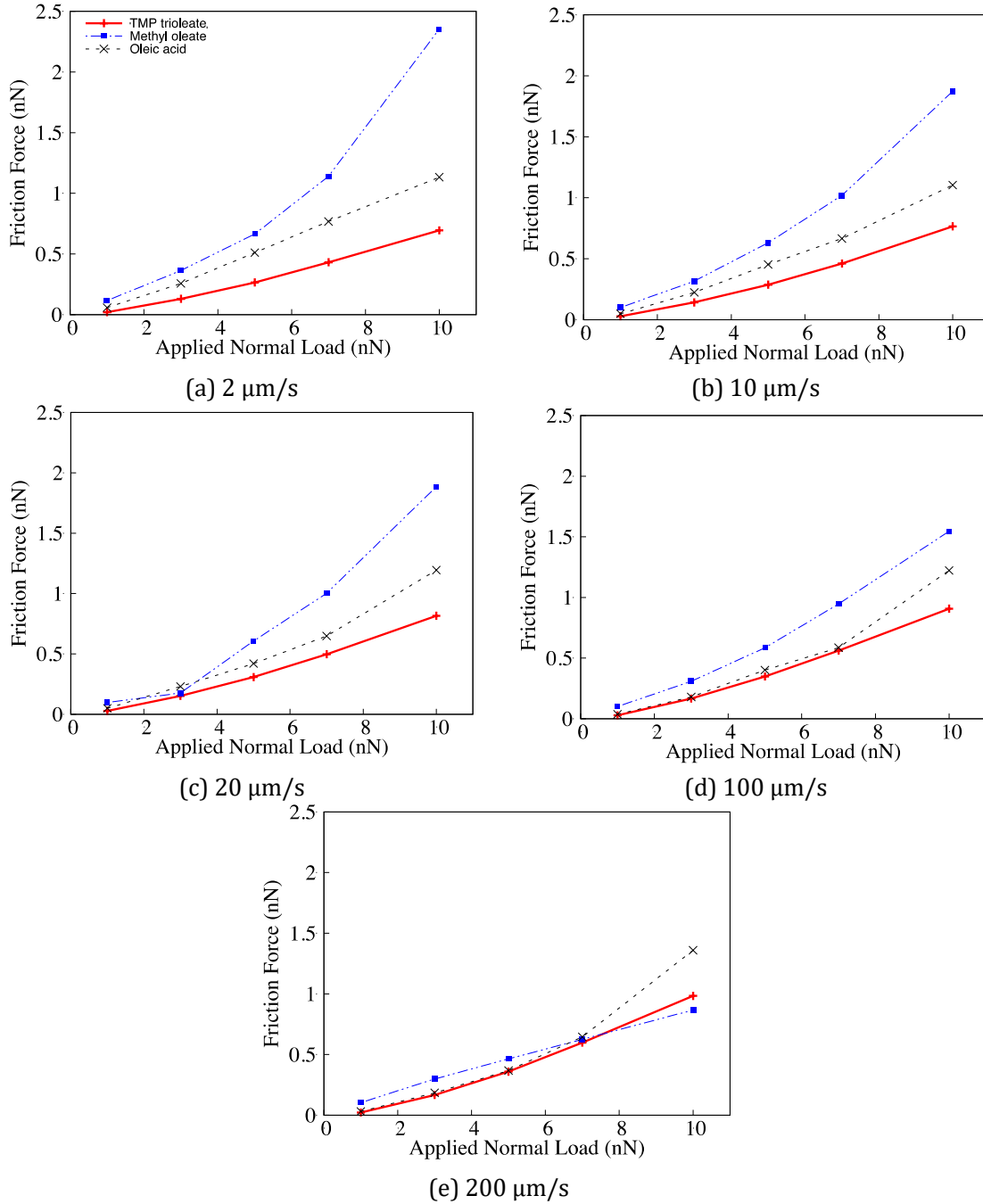
(d) 100 µm/s

(e) 200 µm/s

Figure 6: Friction force vs normal load for tested fluids at different AFM tip sliding speeds.
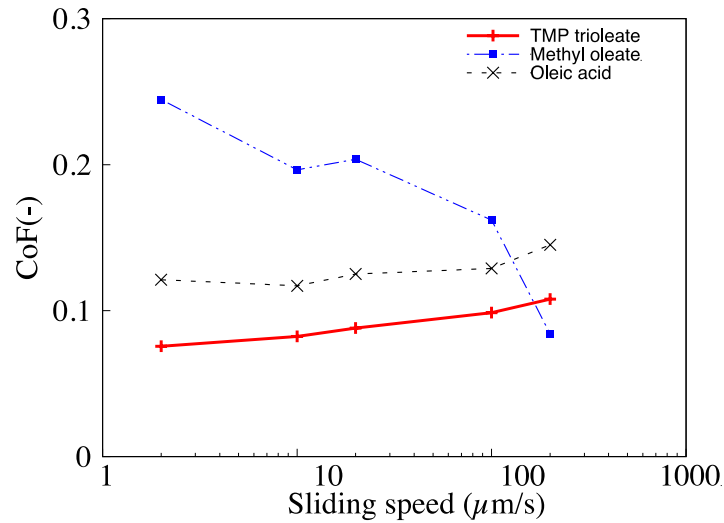
Figure 7: Coefficient of Friction (CoF) for tested fluids at different AFM tip sliding speeds.

Table 2: Averaged thermal activation energy components for tested fluids using LFM.

Type of fluid	Thermal Activation Energy Parameters (kJ/mol)			
	E	Q	$P\Omega$	$\tau\phi$
TMP trioleate	33.78	-15.58	85.39	36.03
Methyl oleate	33.77	10.14	49.68	26.05
Oleic acid	33.77	52.73	-26.06	-7.10

Note: $E = Q + P\Omega - \tau\phi$

On the other hand, oleic acid is shown to have negative values for both the pressure activation ($P\Omega$) and shear activation ($\tau\phi$) energies. The shear activation energy ($\tau\phi$) associates the energy that is required to maintain continuous sliding motion (Hamdan et al., 2018). The negative values of both $P\Omega$ and $\tau\phi$ could be attributed to the tendency of insufficient lubricant entrainment in forming a boundary film for the contact lubricated with oleic acid (Chong and Ng, 2016). The lack of ability to form/provide an effective boundary film could also explain the significantly larger activation energy to initiate sliding (Q) for oleic acid. Even though the CoF is higher (except at 200 µm/s), methyl oleate exhibits a more balanced activation energy characteristic. The activation energies are positive values with potentially a more efficient formation of boundary film. The advantage of such balanced activation energy characteristics could have been attributed to the reducing CoF with higher sliding speeds, indicating that the boundary frictional property of methyl oleate might be shear activated. By comparison, methyl oleate also possesses a sufficiently high enough load carrying capacity ($P\Omega$) with the lowest possible shear resistance ($\tau\phi$), which is in line with the suggestion by Chong et al. (2012), where for an optimised boundary lubrication system, the contact is expected to have sufficient load carrying capacity ($P\Omega$) and low shear behaviour ($\tau\phi$).

CONCLUSION

The present study analysed the boundary lubricity of oleic acid, methyl oleate and TMP trioleate using LFM. The measured CoF for TMP trioleate is the lowest among the tested fluids except at higher sliding speeds of 200 μm/s. However, methyl oleate exhibited a shear activated boundary frictional behaviour, where the CoF reduces with an increase in sliding velocity. The CoF for methyl oleate at 200 μm/s is also found to be the lowest. Such a boundary lubricity characteristic could be attributed to the more balanced activation energy properties as compared to oleic acid and TMP trioleate, resulting in a stronger boundary film that can be better sustained under higher shear rates. Therefore, based on nano-frictional performance, for velocities below 200 μm/s, TMP trioleate generates the lowest CoF, followed by oleic acid and methyl oleate. However, for velocities above 200 μm/s, methyl oleate could potentially form a more stable boundary film due to its more balanced activation energy properties.

REFERENCES

Abd Wafti, N. S., Yunus, R., Lau, H. L. N., Yaw, T. C. S., & Aziz, S. A. (2021). Immobilized lipase-catalyzed transesterification for synthesis of biolubricant from palm oil methyl ester and trimethylolpropane. Bioprocess and Biosystems Engineering, 1-16.

Ahimou, F., Semmens, M. J., Novak, P. J., and Haugstad, G. (2007). Biofilm cohesiveness measurement using a novel atomic force microscopy methodology. Applied and Environmental Microbiology, 73(9):2897–2904.

Aziz, N. A. M., Yunus, R., Rashid, U., and Zulkifli, N. W. M. (2016). Temperature effect on tribological properties of polyol ester-based environmentally adapted lubricant. Tribology International, 93:43–49.

Bongfa, B., Hamid, M. K. A., Samin, P. M., and Adeoti, M. O. (2020). Coconut-castor oil mixture: The potential of flow to tribo-contacts of internal combustion engine at low-temperatures. Journal Tribologi, 27, 132-142.

Briscoe, B. and Evans, D. (1982). The shear properties of langmuir—blodgett layers. Proceedings of the Royal Society of London. A. Mathematical and Physical Sciences, 380(1779):389–407.

Buenviaje, C., Ge, S.-R., Rafailovich, M., and Overney, R. (1998). Atomic force microscopy calibration methods for lateral force, elasticity, and viscosity. MRS Online Proceedings Library Archive, 522.

Chong, W. W. F. and Ng, J.-H. (2016). An atomic-scale approach for biodiesel boundary lubricity characterisation. International Biodeterioration & Biodegradation, 113:34–43.

Chong, W. W. F., Teodorescu, M., & Rahnejat, H. (2012). Physio-chemical hydrodynamic mechanism underlying the formation of thin adsorbed boundary films. Faraday discussions, 156(1), 123-136.

Chong, W.W.F. and Rahnejat, H. (2015). Nanoscale friction as a function of activation energies. Surface Topography: Metrology and Properties, 3(4):044002.

Eyring, H. (1936). Viscosity, plasticity, and diffusion as examples of absolute reaction rates. The Journal of chemical physics, 4(4):283–291.

Fazal, M. A., Haseeb, A. S. M. A., & Masjuki, H. H. (2013). Investigation of friction and wear characteristics of palm biodiesel. Energy conversion and management, 67, 251-256.

Hamdan, S. H., Chong, W. W. F., Ng, J.-H., Chong, C. T., and Zhang, H. (2018). Nano-tribological characterisation of palm oil-based trimethylolpropane ester for application as boundary lubricant. Tribology International, 127:1–9.

Hamdan, S. H., Chong, W. W.F., & Din, M. H. (2018). Frictional analysis on engine lubricant dilution by coconut oil and soybean oil derived biodiesel. Jurnal Tribologi, 18, 149-158.

Hamdan, S. H., Lee, C. T., Lee, M. B., Chong, W. W. F., Chong, C. T., and Sanip, S. M. (2021). Synergistic nano-tribological interaction between zinc dialkyldithiophosphate (ZDDP) and methyl oleate for biodiesel-fueled engines. Friction, 9(3), 612-626.

Hamrock, B. J., Schmid, S. R., & Jacobson, B. O. (2004). Fundamentals of fluid film lubrication. CRC press.

Jackson, M., and Morrell, J. (2011). Tribology in manufacturing. In Tribology for Engineers (pp. 161-241). Woodhead Publishing.

Jahanmir, S., and Beltzer, M. (1986). Effect of additive molecular structure on friction coefficient and adsorption.

Jiang, S., Li, S., Liu, L., Wang, L., and Mominou, N. (2015). The tribological properties and tribochemical analysis of blends of poly alpha-olefins with neopentyl polyol esters. Tribology International, 86:42–51.

Kržan, B. and Vižintin, J. (2003). Tribological properties of an environmentally adopted universal tractor transmission oil based on vegetable oil. Tribology International, 36(11):827–833.

Leighton, M., Nicholls, T., De la Cruz, M., Rahmani, R., and Rahnejat, H. (2017). Combined lubricant–surface system perspective: Multi-scale numerical–experimental investigation. Proceedings of the Institution of Mechanical Engineers, Part J: Journal of Engineering Tribology, 231(7):910–924.

Mahmud, H. A., Salih, N., & Salimon, J. (2015). Oleic acid based polyesters of trimethylolpropane and pentaerythritol for biolubricant application. Malaysian Journal of Analytical Sciences, 19(9).

McDermott, M. T., Green, J.-B. D., and Porter, M. D. (1997). Scanning force microscopic exploration of the lubrication capabilities of n-alkanethiolate monolayers chemisorbed at gold: structural basis of microscopic friction and wear. Langmuir, 13(9):2504–2510.

Odi-Owei, S. (1989). Tribological properties of some vegetable oils and fats. Lubr. Eng, 45(11):685–690.

Overney, R., Tyndall, G., and Frommer, J. (2004). Kinetics and energetics in nanolubrication. Springer handbook of nanotechnology. Berlin: Springer-Verlag, 2004:883–96.

Pandey, A. K., Nandgaonkar, M., & Suresh, S. (2020). Comparison and Evaluation of Engine Wear, Performance, NOx Reduction and Nano Particle Emission of Diesel, Karanja and Jatropha Oil Methyl Ester Biodiesel in a Military720 kW, heavy duty CIDI Engine Applying EGR with Turbo Charging (No. 2020-01-0618). SAE Technical Paper.

Rani, S., Joy, M., and Nair, K. P. (2015). Evaluation of physiochemical and tribological properties of rice bran oil–biodegradable and potential base stoke for industrial lubricants. Industrial Crops and Products, 65:328–333.

Ranjan, N., Shende, R. C., Kamaraj, M., & Ramaprabhu, S. (2021). Utilization of TiO 2/gC 3 N 4 nanoadditive to boost oxidative properties of vegetable oil for tribological application. Friction, 9(2), 273-287.

Rudnick, L. R. (2005). Synthetics, mineral oils, and bio-based lubricants: chemistry and technology. CRC press.

Shahabuddin, M., Mofijur, M., Kalam, M. A., & Masjuki, H. H. (2020). Study on the friction and wear characteristics of bio-lubricant synthesized from second generation jatropha methyl ester. Tribology in Industry.

Shashidhara, Y. and Jayaram, S. (2010). Vegetable oils as a potential cutting fluid—an evolution. Tribology international, 43(5-6):1073–1081.

Spikes, H. (2018). Stress-augmented thermal activation: Tribology feels the force. Friction, 6(1):1–31.

Srinivas, V., Chebattina, K. R. R., Pranay, G. V. S., Lakkoju, B., & Vandana, V. (2020). Tribological properties of polyol ester–commercial motorbike engine oil blends. Journal of King Saud University-Engineering Sciences.

Sripada, P. K., Sharma, R. V., and Dalai, A. K. (2013). Comparative study of tribological properties of trimethylolpropane-based biolubricants derived from methyl oleate and canola biodiesel. Industrial Crops and Products, 50:95–103.

Subhalakshmi, K., Devaprakasam, D., Math, S., and Biswas, S. (2008). Use of eyring equation to explore the frictional responses of a–cf 3 and a–ch 3 terminated monolayers self-assembled on silicon substrate. Tribology Letters, 32(1):1.

Umer, J., Morris, N., Rahmani, R., Balakrishnan, S., and Rahnejat, H. (2020). Nanoscale frictional characterisation of base and fully formulated lubricants based on activation energy components. Tribology International, 144:106115.

Yunus, R., Rasheed, H. S., and Zulkifli, N. W. M. (2020). Wear and friction behavior of semi synthetic engine oil blended with palm oil/TMP ester and nano glass powder additive. Jurnal Tribologi, 26, 16-36.

Zulkifli, N., Azman, S., Kalam, M., Masjuki, H. H., Yunus, R., and Gulzar, M. (2016). Lubricity of bio-based lubricant derived from different chemically modified fatty acid methyl ester. Tribology International, 93:555–562.

Zulkifli, N., Masjuki, H., Kalam, M., Yunus, R., and Azman, S. (2014). Lubricity of bio-based lubricant derived from chemically modified jatropha methyl ester. Journal Tribologi, 1:18–39.